International Journal of Environmental Science and Technology (2023) 20:13783–13798
https://doi.org/10.1007/s13762-023-04935-4

ORIGINAL PAPER

Soda residue as a novel modifier for straw biochar enhanced recovery of phosphate and ammonium from water

L. Liu[1] · M. Zhang[1]

Received: 31 October 2022 / Revised: 28 February 2023 / Accepted: 10 April 2023 / Published online: 25 April 2023

Abstract

A novel adsorbent was prepared by co-pyrolysis of industrial soda residue and straw powder at mass ratio of 2:1 (SRB 2:1) for efficient recovery of phosphate (PO_4^{3-}) and ammonium (NH_4^+) from water. The maximum adsorption capacity of SRB 2:1 toward PO_4^{3-} and NH_4^+ reached 114.96 and 3.87 mg/g, which were about 80 and 1.7 times than that of raw straw biochar, respectively. Based on the adsorption thermodynamic results, phosphate adsorption was spontaneous ($\Delta G^\circ < 0$) and endothermic ($\Delta H^\circ > 0$) so that increasing temperature could promote the adsorption process. The dominant mechanisms of phosphate removal included surface precipitation, ligand exchange, and electrostatic attraction. SRB 2:1 exhibited excellent performance on removing nutrients from real domestic wastewater, particularly with 95% removal for phosphate. Pot experiment showed that post-adsorption SRB 2:1 as a slow-releasing fertilizer promoted growth of wheat seeds. This study indicated that straw biochar modified by industrial soda residue was efficient in reclaiming nutrients as fertilizer, providing a new possibility of nutrients recovery and solid wastes recycling.

Keywords Biochar · Soda residue · Phosphate · Ammonium · Adsorption · Recovery

Introduction

Excessive discharge of nutrients (i.e., phosphorus, nitrogen) has led to the eutrophication of natural water which can cause the depletion of dissolved oxygen, algal reproduction and death of aquatic organisms (Banu et al. 2019). Also, it threatens the safety of drinking water and the biodiversity of aquatic ecosystem (Zhang et al. 2013). Eutrophication occurs when phosphorus and nitrogen content of water exceed 0.02 mg/L and 0.3 mg/L, respectively (Yao et al. 2013), which has become a major environmental issue for the moment. Therefore, efficient removal of phosphorus and nitrogen from water is extremely important to prevent eutrophication and maintain the health of aquatic ecosystem (Xi et al. 2022). Furthermore, the recovery of phosphorus and nitrogen from wastewater will be a promising method, which can not only control eutrophication, but also reclaim nutrients for further possible application as fertilizer (Shakoor et al. 2021).

At present, many technologies and methods have been applied to remove phosphorus and nitrogen, including electrodialysis, ion exchange, precipitation and bio-transformation (Zhang et al. 2020b). However, many disadvantages (e.g., low removal efficiency, potential secondary pollution, and high operation and maintenance costs) hinder their large-scale application (Cai and Ye 2022). In contrast, adsorption is an efficient and economical method for removing nutrients from water (Zhang et al. 2020a). Many materials were used as adsorbents including activated carbon, graphene, chitosan and biochar (An et al. 2021; McGinley et al. 2022; Xu et al. 2022; Zhang et al. 2022). Recently, the adsorption of nutrients via biochar has posed extensive attention, due to its high-efficiency and environmental friendliness (Xu et al. 2018). Biochar is a porous, hydroxy-rich and high-carbon solid material produced from the high-temperature pyrolysis process of organic materials (e.g., straw, fruit shell, food waste, plant stalk and animal manure) in oxygen-limited or anoxic environments (Feng et al. 2022). In addition, the application of biochar can increase agricultural productivity, clean wastewater and help reduce the use of chemical fertilizers. However, due to the low adsorption ability for

Editorial responsibility: Nour Sh. El-Gendy.

✉ M. Zhang
stu_zhangml@ujn.edu.cn

[1] School of Water Conservancy and Environment, University of Jinan, Jinan 250022, China

anionic pollutants (e.g., phosphate), it would be necessary to modify raw biochar for improving its adsorption capacity.

So far, many studies showed that the modification method of raw biochar by loading metal ions could enhance phosphate adsorption ability. For instance, Zhang et al. (Zhang et al. 2021) studied the use of $La(OH)_3$-supported biochar to remove phosphate from water with a maximum phosphate adsorption capacity of 116.08 mg/g. Xi et al. (Xi et al. 2022) demonstrated that Mg-doped biochar/bentonite composite beads could concurrently remove phosphate (132.2 mg/g) and nitrogen (39.5 mg/g) from wastewater and the spent composites could be used as fertilizer to recycle. The adsorption mechanism was attributed to the formation of struvite crystallization. Zhuo et al. (Zhuo et al. 2022) recently used calcium-modified corn stover biochar to achieve simultaneous adsorption of phosphate and tetracycline, and the adsorption capacities of modified biochar toward phosphate and tetracycline were up to 33.94 and 33.53 mg/g, respectively. Li et al. (Li and Shi 2022) explored the adsorption possibility of iron- and nitrogen-modified biochar and successfully removed tetracycline, ammonium and phosphate from the swine sewage. Tran et al. (Phuong Tran et al. 2022) developed an aluminum-modified biochar to remove simultaneously nitrate and phosphate with the maximum adsorption capacities of 26.67 mg N/g and 78.99 mg P/g, respectively.

Although these biochars modified by loading metal ions (e. g. La, Mg, Ca, Fe, Al) exhibited good performance in phosphate and nitrogen removal from aqueous solution, there are still many disadvantages (e.g., secondary pollution, high cost) on chemical reagents modification method. Recently, the biochar modified by metal-containing solid wastes (e.g., distiller grains, phosphogypsum, coal gangue and dolomite) has attracted intensive attention due to their low cost and recycling for resources (Li et al. 2019; Lian et al. 2019; Qiu and Duan 2019). Therefore, the application of low-cost modified biochar prepared by solid waste may be promising alternative for adsorption in the future (Xue et al. 2021).

As a solid waste discharged from the production process of ammonia-soda, soda residue mainly consists of calcium carbonate, calcium sulfate and a small amount of magnesium salts. Soda production in China has reached about 4.2 million tons per year and 1.5 million tons soda residue will be produced every year. Currently, most of soda residue were piled up and deposited on the ground, which could result in the land salinization and contamination to the soil and aqueous environment, due to its strong alkalinity (pH 10–12). Also, soda residue particle is extremely small so that can be easily inhaled into body to harm human health. Therefore, it is very urgent to properly treat soda residue for maintaining the safety of eco-environment system, particularly for realizing the resource reutilization of soda residue. As a Ca/Mg-rich solid waste, soda residue has potential possibility to modify raw biochar for enhancing the adsorption capacity of pollutants. To our knowledge, no systematic study has been reported on the application of industrial soda residue as modifier to improve the recovery of phosphate and ammonium from water.

In this study, a novel synthetic material was prepared via co-pyrolysis of industrial soda residue and sorghum straw powder. The objectives of this study were to: (1) explore the recovery possibility of phosphorus and nitrogen by soda residue-modified biochar composites; (2) reveal the adsorption behavior and mechanisms of the synthetic biochar composite toward phosphate and ammonium; (3) assess the effect of post-adsorption biochar for wheat seedlings growth.

Materials and methods

Materials

The soda residue was collected from a soda production factory in Weifang city, Shandong Province, which was generated during the production process of ammonia-soda. Sorghum straw was obtained from one farm and washed several times with deionized (DI) water to remove impurities on the surface and dried in an oven at 95 °C for 24 h. Both materials were grinded and screened with a 100-mesh sieve. All chemical reagents used for the experiments are analytical reagents grade. DI water was used in all experiments. Phosphate stock solution (500 mg/L) was prepared by dissolving 2.197 g KH_2PO_4 into 1000 mL DI water and stored at 4 °C.

Preparation of experimental materials

The soda residue and sorghum straw powders were placed in a tubular furnace (OTF-1200X, Jing, China) to prepare the Ca-doped biochar composite. Both were evenly mixed (at the mass ratio of 1:0, 1:2, 1:1, 2:1 and 0:1) and the modified biochar was obtained by pyrolyzing for 2 h at 800 °C with a rate of 10 °C/min (Fig. 1). Then, the collected samples were filtered with DI water for 2–3 times and dried for 12 h at 105 °C. The synthetic materials (at mass ratio of soda residue to sorghum straw powder 1:0, 1:2, 1:1, 2:1 and 0:1) were labeled as SR, SRB 1:2, SRB 1:1, SRB 2:1 and BC, respectively. The synthetic materials were ground through a 100-mesh sieve and stored for use.

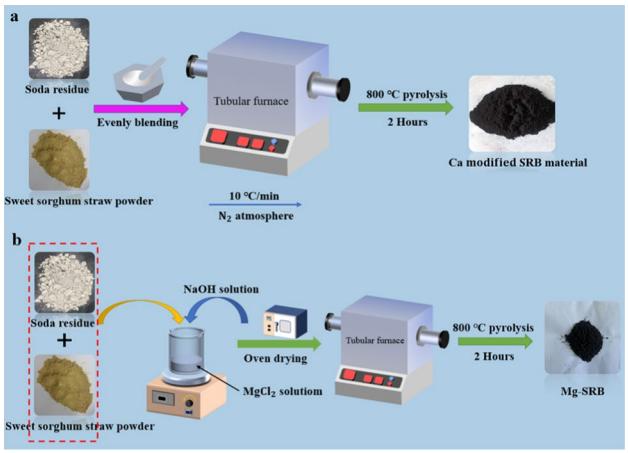

Fig. 1 The preparation process of SRB materials (**a**) and Mg-SRB (**b**)

Some literature reported that Mg-modified biochar exhibited excellent adsorption ability to phosphate by Mg-P precipitate formation (Cai and Ye 2022; Shakoor et al. 2021; Xi et al. 2022; Zhang et al. 2020b). Hence, to compare the phosphate adsorption ability of SRB 2:1 and Mg-laden SRB 2:1, Mg^{2+} laden biochar was prepared by the following methods. 12 g mixture of soda residue and sorghum straw powder (at mass ratio 2:1) was added into the solution containing 200 mL $MgCl_2{\cdot}7H_2O$ (0.738 mol/L). After mixing for 1 h, the pH was adjusted by adding the diluted NaOH solution. Afterward, the obtained substance was aged for 24 h at 85 °C. After the supernatant being evaporated, the residue slurry was filtered with DI water for 2–3 times and placed in an oven to dry overnight at 105 °C. The obtained material was pyrolyzed with the same method described above. The synthetic composite biochar was ground and screened with a 100-mesh sieve and marked as Mg-SRB.

Characterization of biochars

The characterizations of surface structure and composition of all synthetic materials were performed by scanning electron microscope (SEM, Tescan Mira Lms, Czech) equipped with energy-dispersive X-ray spectrometer (EDS), X-ray diffractometer (XRD, Ultima IV, Japan), Fourier transform infrared spectroscopy (FTIR, FTS-165, PerkinElmer, USA) and surface area analyzer (ASAP 2460, USA).

Batch adsorption experiments

Batch adsorption experiments, including effects of solution pH, adsorption isotherms, adsorption kinetics, adsorption thermodynamic and co-existing anion competition experiments, were conducted in this study. All batch experiments were conducted in 50-mL polyethylene bottles at room temperature 25 °C with oscillation speed (120 r/min) and adsorbent dosage of 1.67 g/L. The ammonium molybdate spectrophotometric method was used to measure phosphate concentration.

The influence of initial solution pH on adsorption process was performed by adjusting the pH to 2–11. After passed through 0.45-μm filter paper, the phosphate concentrations of filtrate were measured. Meanwhile, the electrical conductivity (EC) and final pH of the filtrate after phosphate adsorption were measured to analyze the variation of physicochemical property of solutions. For adsorption isotherm experiment, 0.05 g adsorbent was added to 30 mL solution with different phosphate concentrations (50–400 mg P/L). To investigate the influence of different temperatures for the adsorption reaction, the adsorption isotherm experiment was conducted at 318 K, 298 K and 277 K, respectively. To study adsorption kinetics, 0.15 g SRB 2:1 material was put into 90 mL solutions (100 mg P/L and 200 mg P/L), and samples were collected at 5–1440 min and filtered for measurement. For exploring the effect of co-existing anions (i.e., CO_3^{2-}, SO_4^{2-}, HCO_3^- and NO_3^-) on phosphate adsorption, the anions with different concentrations were used to conduct co-existing anionic competition experiments.

Removal of ammonium

To investigate the feasibility of ammonium removal on SRB 2:1, the effect of initial ammonium concentrations and initial pH were performed at room temperature. Ammonium solution was obtained by dissolving NH_4Cl into DI water, and its concentration was measured by Nascent reagent spectrophotometric method. The effect of solution pH on ammonium removal was conducted by adding 0.05 g adsorbents (BC, Mg-SRB, SRB 2:1) into 30 mL ammonium solution (10 mg N/L) with a pH range from 2 to 11. The effect of different ammonium concentrations (2–20 mg N/L) was performed at pH 9. After being shaken (120 r/min) for 24 h, the mixture was filtered through 0.45-μm filter paper. Each group was conducted in triplicate and the average value was presented.

Phosphate removal of real domestic wastewater

To evaluate the performance of phosphate and ammonium removal from real domestic wastewater, 0.15 g biochar (SRB 2:1) was added into 90 mL real domestic wastewater with oscillation (120 r/min) at 25 °C for 2 h. After treatment, the mixture was filtered through 0.45-μm filter paper for water quality analysis (e.g., pH, Eh, COD, NH_4^+, TP, PO_4^{3-} and NO_3^-).

Pot experiment

To assess the feasibility of nutrients recovery of post-adsorption SRB 2:1, pot experiment was conducted by using post-adsorption SRB 2:1 material as slow-releasing fertilizer. Four treatment groups were applied to pot experiment: 300 g raw soil; 300 g raw soil + 3 g commercial fertilizer; 300 g raw soil + 3 g SRB 2:1; and 300 g raw soil + 3 g SRB 2:1 after adsorption. Wheat seeds were immersed in DI water for 24 h before planting. Then 20 wheat seeds were evenly placed in the soil, which was maintained in the same external environment. The germination and growth of wheat seeds were observed every day. After 20-day wheat cultivation, the wheat seedlings were harvested for dry and wet weight analysis to evaluate the nutrients slow-releasing ability of post-adsorption SRB 2:1 compared with commercial fertilizer. In addition, chemical properties of the soil (pH, EC) were measured to investigate the effect of biochar on soil quality.

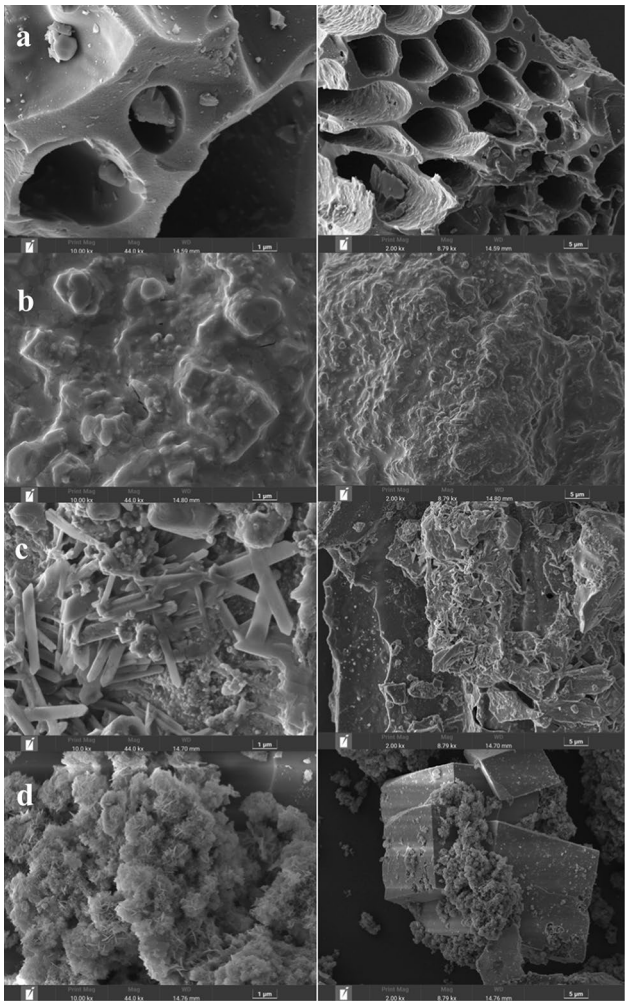

Fig. 2 The SEM images of straw biochar (BC) (**a**), pyrolyzed soda residue (SR) (**b**), soda residue modified straw powder at mass ratio of 2:1(SRB 2:1) (**c**), and post-adsorption SRB 2:1 (**d**)

Results and discussion

Characterization analysis

The surface structure and morphology of BC, SR, and SRB 2:1 are described by SEM images (Fig. 2). There are many large and deep pores on the surface of BC due to the release of pyrolysis gas at 800 °C, resulting in the highest S_{BET} among all biochars (Table 1). There were many irregular particles on the surface of SR (Fig. 2b), which may be attributed to the generation of metal oxides (e.g., MgO, CaO) during the process of high-temperature pyrolysis. Compared with porous structure of BC, many prismatic crystals and flocculent particles were distributed on the surface of SRB 2:1, suggesting that metal elements of soda residue were attached to the surface of biochar after modification. It indicated that the interaction between biomass and soda residue during co-pyrolysis process directly affected physicochemical properties, element composition and specific surface area of the biochar composite (Wang et al. 2021).

The physicochemical properties (e.g., pH, pH_{pzc}, S_{BET} and pore size) of the biochars are listed in Table 1. The pH of all biochar composites was alkaline. Compared with the pH of raw biochar (10.85), soda residue-modified biochar increased to more than 12 due to the formation of calcium oxide during the pyrolysis process. The zero potential (pH_{pzc}) of modified biochars was higher than that of raw biochar (Online Resource 4), suggesting that modified biochar had better phosphate adsorption ability relying on the electrostatic attraction. The pH_{pzc} of soda residue-modified biochar all exceeded 10, which would greatly boost the adsorption capacity of anionic pollutants at wide pH range (Mitrogiannis et al. 2017).

Table 1 Physicochemical properties of different biochars

Biochar	S_{BET} (m^2/g)	Pore volume (cm^3/g)	Pore size (nm)	pH_{pzc}	pH
BC	399.52	0.220	2.24	8.59	10.85
SRB 1:2	92.74	0.066	2.83	10.30	12.44
SRB 1:1	56.36	0.041	2.89	10.73	12.46
SRB 2:1	5.48	0.094	6.89	10.86	12.30
SR	2.60	0.009	13.24	10.43	11.85
Mg-SRB	27.81	0.066	9.45	10.48	11.65

The nitrogen adsorption–desorption isotherms of all biochars are shown in Online Resource 1. It indicated that the N_2 adsorption–desorption isotherms of modified biochars could be considered as type IV isotherm, which were similar to many mesopores industrial adsorbents (Sing 1982). Seen from Table 1, the S_{BET} of BC was high as 399.52 m^2/g and that of modified biochars decreased with increasing in the mass proportion of soda residue. In contrast, pore size of modified biochars became larger with the mass proportion of soda residue increasing. Many gases (e.g., CO_2) were discharged during high-temperature pyrolysis of raw materials, thus enlarged the pore size of modified biochars. Meanwhile, the generated metal oxides (e.g., CaO, MgO) could embed in the pore of the biochar, which caused blockage of the pore.

Seen from Fig. 3, the FTIR peak at 3444 cm^{-1} was assigned to the stretching vibration peaks of O–H (Zhao et al. 2020). The peaks at 1650 cm^{-1} and 1450 cm^{-1} were ascribed to the C=O stretching vibrations of carboxyl and aromatic C=C stretching vibrations, respectively (Ahmad et al. 2012; Feng et al. 2022). The increase of oxygen-containing functional groups will be beneficial to remove phosphate via ligand exchange (Feng et al. 2022). Especially, the vibration peaks at 1425 cm^{-1} represented inorganic CO_3^{2-} (Fang et al. 2014), and the peak area of CO_3^{2-} gradually increased with the enhancement of soda residue proportion in the mixture. The peaks at around 858 cm^{-1} and 781 cm^{-1} were the vibration bands of aromatic C–H (Ismail and Hameed 2014; Munar-Florez et al. 2021; Zhang et al. 2018). The peaks at 985 cm^{-1} and 905 cm^{-1} could be attributed to formation of Ca/Mg–O (Zhang et al. 2018), which could further improve the adsorption ability of phosphate on Mg-SRB. Compared with raw biochar, the functional groups of modified biochar significantly increased due to the addition of soda residue, suggesting the adsorption ability of the modified biochar would be improved.

The XRD pattern of raw soda residue is presented in Online Resource 3. The peaks at 23.1°, 29.4°, 36.0°, 39.4°, 43.1°, 47.5°, 48.5°, 57.4°, 60.7° and 64.7° represented $CaCO_3$, and the peaks at 11.7°, 14.76°, 20.8°, 23.4°, 25.68° and 28.14° belonged to $CaSO_4$ (i.e., $CaSO_4{\cdot}0.5H_2O$ and $CaSO_4{\cdot}2H_2O$). The results indicated that the main component of raw soda residue was Ca-laden compound. The XRD patterns of different biochars are presented in Fig. 4. The peaks at 2θ = 22.6° and 43.06° were ascribed to amorphous carbon (002) and graphite carbon (101) which were the characteristic peaks of plant-based biochar (Duan et al. 2015; Li et al. 2020). The diffraction peaks at 2θ = 31.66°, 45.24°, 49.42°, 56.1°, 65.76°, 74.62° and 83.22° were attributed to CaS, which was produced during the 800 °C co-pyrolysis of calcium sulfate from soda residue and carbon from sorghum straw. The peaks at 2θ = 26.76° and 36.64° represented CaO and those at 2θ = 18.02°, 26.66°, 28.14°, 32.3°, 38.36°, 47.04°, 50.7°, 55.88° and 60.82° were attributed to CaClOH. In addition, the peaks of MgO could be observed at 2θ = 37.24°, 42.96°, 62.5° and 78.7°. The results suggested that the metal cations (Ca and Mg) have been successfully embedded into the modified biochar, which would

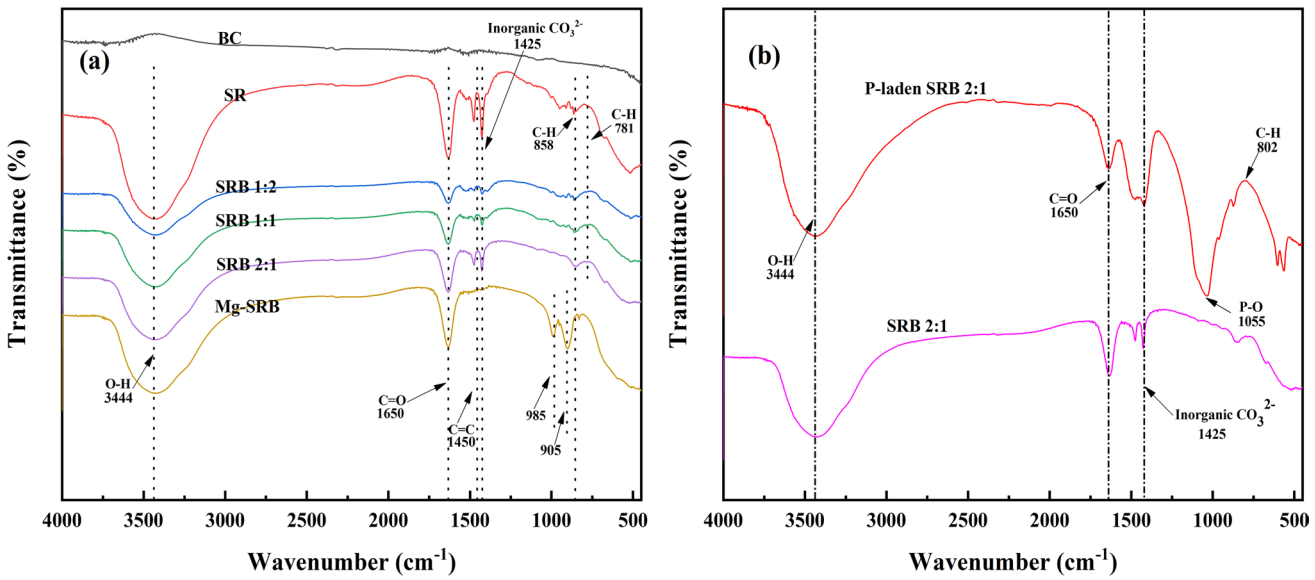

Fig. 3 FTIR spectra of the biochars (**a**) and post-adsorption SRB 2:1 (**b**)

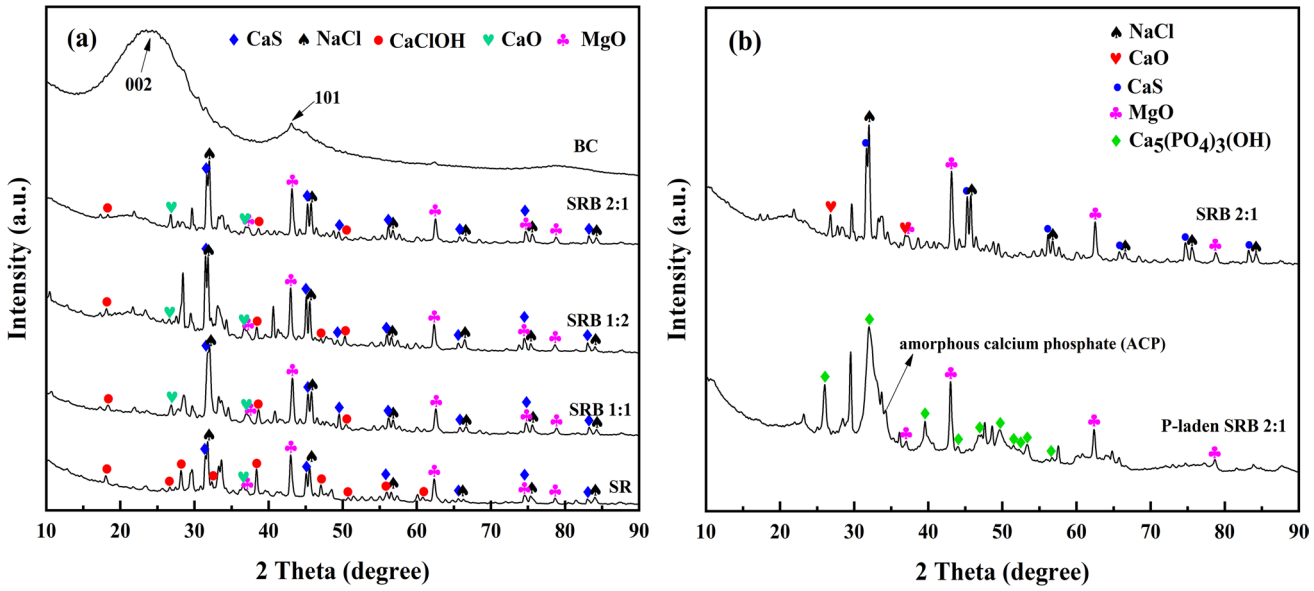

Fig. 4 XRD pattern of the biochars (**a**) and post-adsorption SRB 2:1 (**b**)

significantly boost the removal efficiency of phosphate by surface precipitation.

Effect of pH

It is important to study the effect of solution pH on phosphate adsorption process, as pH can affect the surface charge of biochar and the degree of adsorbate ionization (Wang et al. 2020). Seen from Fig. 5, the modified biochars showed very high removal capacities of phosphate at lower initial concentrations (50–100 mg P/L) with a wide pH range of 2.0–11.0, and initial solution pH had minor impact on their adsorption capacities. With the concentration of phosphate enhanced to 200 mg P/L, the modified biochars still kept high removal abilities, but different pH had significant effect on phosphate adsorption, especially SRB 2:1. Seen from Fig. 5c, with the pH increased from 2.0 to 5.0, the adsorption capacity of SRB 2:1 gradually raised, and at pH 5.0 it was up to 127.4 mg P/g, which was the highest among the pHs. The anionic forms of phosphate were mainly $H_2PO_4^-$ and HPO_4^{2-} under acidic aqueous (Chen et al. 2012), thus the positive charges on the surface of SRB 2:1 could rapidly combine with $H_2PO_4^-$ and HPO_4^{2-} by electrostatic attraction and increased removal ability of phosphate. When the solution pH increased to over the pH_{pzc} of SRB 2:1, the modified biochar was deprotonated and negatively charged, which hardly integrated with PO_4^{3-} via electrostatic attraction (Xu et al. 2017), resulting in lower adsorption capacity of phosphate compared with the acidic aqueous. All modified biochars exhibited excellent adsorption abilities of phosphate under different pH conditions, which was mainly attributed to the surface precipitation (e.g., hydroxyapatite) of calcium and phosphate (Mia et al. 2017). In conclusion, compared with BC, modified biochars exhibited good adsorption ability of phosphate with a wide pH scope of 2.0–11.0, especially for SRB 2:1.

The final pH of solution after phosphate adsorption showed an upward trend and reached around 10.0 (Online Resource 2a), which may be attributed to the ligand exchange process between phosphate in the solution and hydroxyl groups from the biochar. Moreover, the change interval between initial pH and final pH in acidic aqueous was larger than that in alkaline aqueous, suggesting that the acidic medium was conducive to introduce more hydroxides into aqueous solution so that further promoted ligand exchange process. Online Resource 2b shows that the EC of the solution (SRB 2:1) was the highest among the solutions. This was associated with the release of more free metal ions (Ca^{2+}) from SRB 2:1.

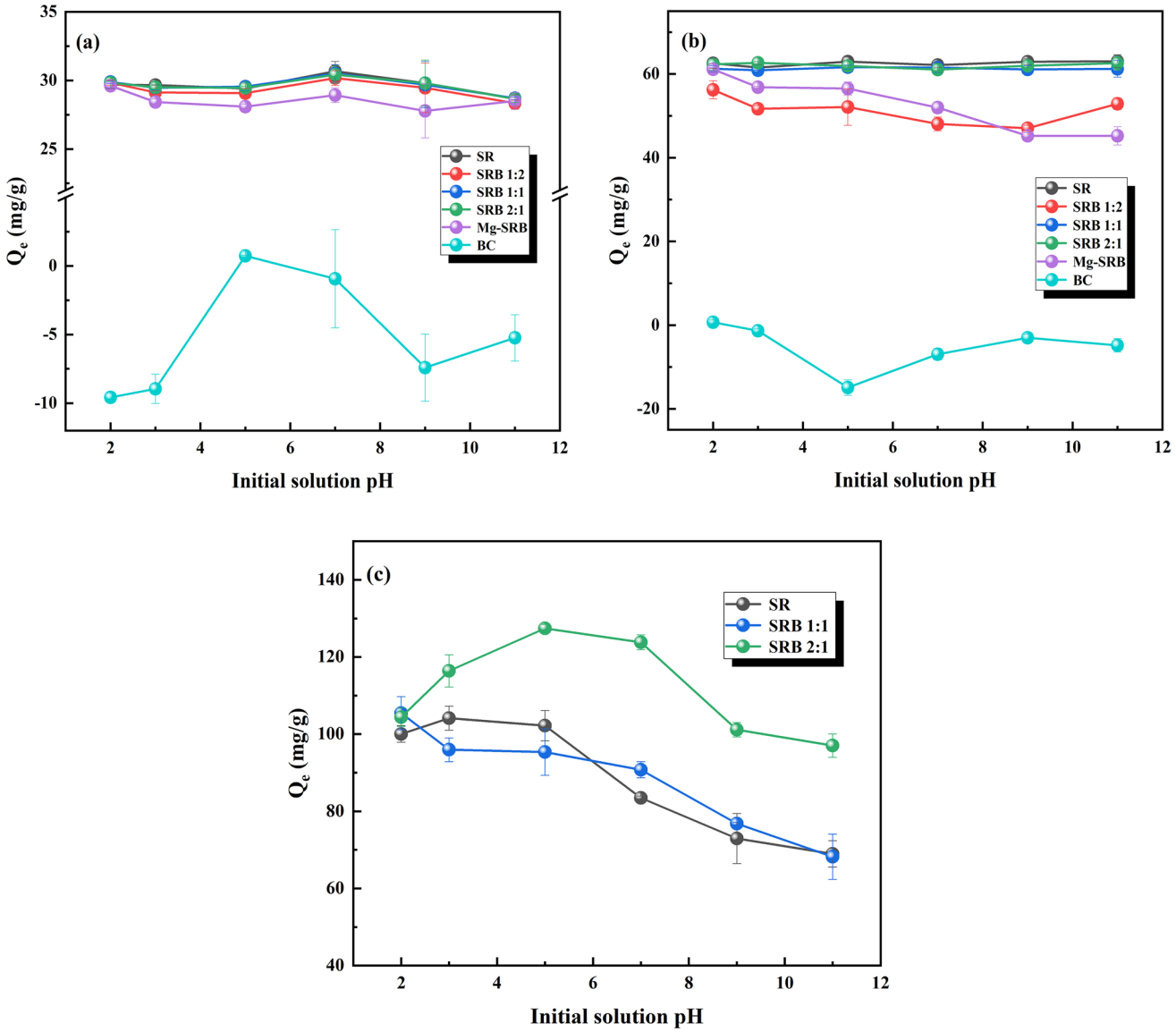

Fig. 5 Effect of initial pH for phosphate adsorption onto different biochars at different phosphorus concentrations: **a** 50 mg P/L; **b** 100 mg P/L; **c** 200 mg P/L

Adsorption isotherms

The phosphate adsorption isotherms of all biochars are shown in Fig. 6. The relevant parameters of isotherms are listed in Table 2. The Langmuir and Freundlich adsorption models are given as follows:

Langmuir model:

$$Q_e = Q_m K_L C_e / \left(1 + K_L C_e\right) \tag{1}$$

Freundlich model:

$$Q_e = K_F C_e^{1/n} \tag{2}$$

where C_e (mg/L) and Q_e (mg/g) represent the solution concentration and the adsorption capacity, respectively, when the adsorption reaction reaches equilibrium; Q_m (mg/g) is the maximum adsorption capacity; K_L is a parameter that Langmuir model characterizes the affinity between adsorbent and adsorbate; K_F is a constant that Freundlich model describes the adsorption capacity of adsorbent; 1/n is a constant related with the Freundlich isotherm change trend.

The Langmuir model supposes that the surface of adsorbent is homogeneous and monolayer adsorption occurs,

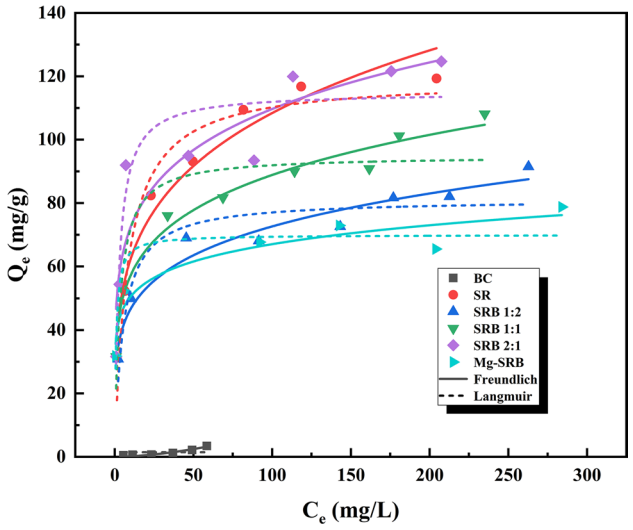

Fig. 6 Adsorption isotherms of the different biochars

while the Freundlich model assumes that the surface of biochar is heterogeneous and multilayer adsorption happens (Kong et al. 2018; Zhang et al. 2020c). As shown in Fig. 6, the adsorption capacity of phosphate on modified biochar continuously enhanced with the initial concentration increase and finally maintained stability. This was because the active adsorption sites on the surface of modified biochar were gradually occupied and until fully saturated. Seen from Table 2, the correlation coefficient (R^2) of the Langmuir model was larger than that of the Freundlich model, suggesting that adsorption performance of phosphate on the modified biochar fitted well the Langmuir model. Thus, the adsorption process of modified biochars could be considered as a monolayer adsorption. The Q_m of phosphate onto raw biochar (BC) was low (1.46 mg P/g), while the Q_m of modified biochar was significantly increased. The Q_m of SRB 2:1 was up to 114.96 mg P/g, which was about 80 times than

Table 2 Adsorption isotherm parameters of phosphate on different biochars

Biochar	Langmuir model			Freundlich model		
	K_L (L/mg)	Q_m (mg/g)	R^2	K_F ($mg^{(1-1/n)}$ $L^{1/n}$/g)	1/n	R^2
BC	/	1.46	/	0.003	1.69	0.90
SR	0.12	119.18	0.97	35.62	0.24	0.96
SRB 1:2	0.19	81.18	0.95	29.83	0.19	0.87
SRB 1:1	0.31	94.90	0.98	36.67	0.19	0.87
SRB 2:1	0.37	114.96	0.91	47.60	0.18	0.86
Mg-SRB	1.13	69.96	0.95	38.07	0.12	0.93

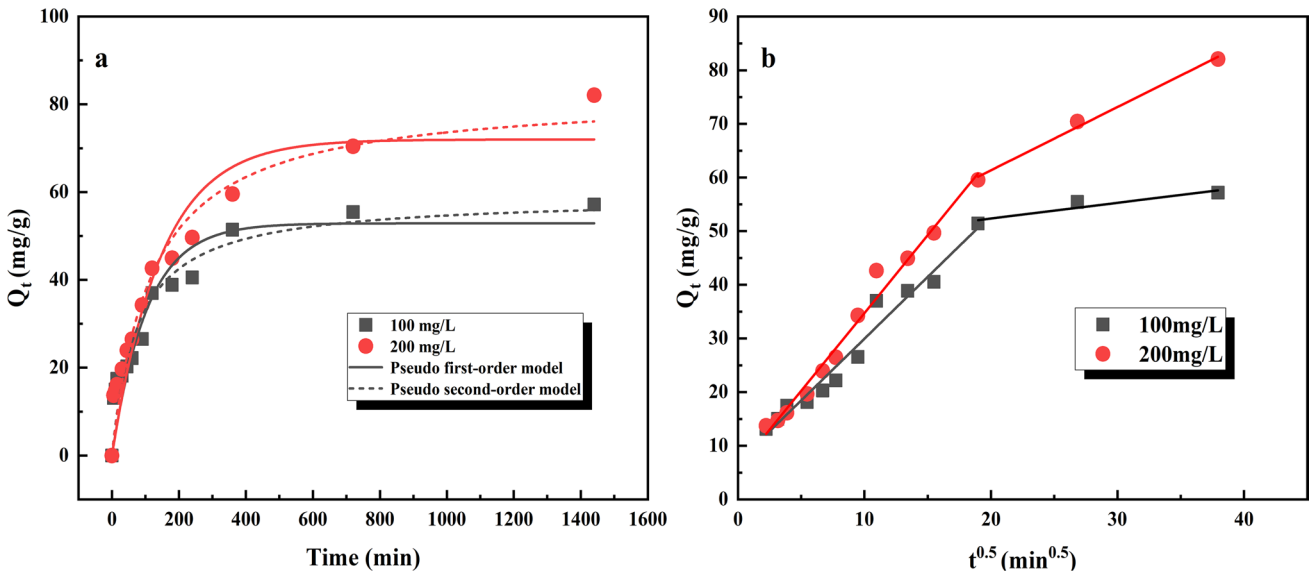

Fig. 7 Adsorption kinetics models of phosphate on SRB 2:1: pseudo-first-order and pseudo-second-order models (**a**); and intra-particle diffusion model (**b**)

Table 3 Adsorption kinetic parameters of phosphate on SRB 2:1 material

Phosphate concentration	Pseudo-first-order model			Pseudo-second-order model			Intra-particle diffusion model					
	k_1 (min^{-1})	Q_e (mg g^{-1})	R^2	k_2 (g mg^{-1} min^{-1})	Q_e (mg g^{-1})	R^2	k_{i1} (mg g^{-1} $min^{-1/2}$)	C_1 (mg g^{-1})	k_{i2} (mg g^{-1} $min^{-1/2}$)	C_2 (mg g^{-1})	R_1^2	R_2^2
100 mg/L	0.009	52.89	0.88	0.0002	58.87	0.92	2.3	6.91	0.29	46.5	0.97	0.90
200 mg/L	0.007	72.0	0.91	0.0001	82.44	0.95	2.9	5.72	1.18	37.8	0.98	0.99

Table 4 Thermodynamic parameters of phosphate adsorption on SRB 2:1 material

Biochar	ΔH^0 (kJ/mol)	ΔS^0 (J/mol K)	ΔG^0 (kJ/mol)		
			277 K	298 K	318 K
SRB 2:1	6.93	31.37	−1.76	−2.42	−3.05

that of raw biochar. In addition, the Q_m of Mg-SRB was 69.96 mg P/g, suggesting Mg decoration of SRB 2:1 could not further improve the adsorption ability of phosphate. The R^2 of the Freundlich model on BC was up to 0.90, suggesting that the adsorption performance of BC could be heterogeneous multilayer physisorption (Ma et al. 2020), which was consistent with its larger S_{BET} (Table 1).

Adsorption kinetics

The kinetic behaviors of phosphate adsorption onto SRB 2:1 were assessed by the pseudo-first-order kinetic model (Qi et al. 2020), pseudo-second-order kinetic model (Amin and Chetpattananondh 2019) and intra-particle diffusion model (Tian et al. 2020).

Pseudo-first-order kinetic model:

$$Q_t = Q_e\left[1 - exp.\left(-k_1 t\right)\right] \tag{3}$$

Pseudo-second-order kinetic model:

$$Q_t = k_2 Q_e^2 t / \left(1 + k_2 Q_e t\right) \tag{4}$$

Intra-particle diffusion model:

$$Q_t = k_{ip} t^{1/2} + C \tag{5}$$

where k_1 and k_2 are the rate constants of adsorption kinetic models; k_{ip} is the rate constants of intra-particle diffusion model; C is a constant related to the thickness of the boundary layer; t (min) is the adsorption time; Q_t (mg/g) and Q_e (mg/g) represent the adsorption capacity at time t and equilibrium stage, respectively.

The fitting of adsorption kinetic models is shown in Fig. 7. The fitting kinetic data on SRB 2:1 are listed in Table 3. The adsorption efficiency of phosphate (100 mg P/L and 200 mg P/L) increased rapidly within 100 min and reached equilibrium approximately at 10 h. The adsorption kinetic performance of phosphate on SRB 2:1 was more in line with the pseudo-second-order model, due to the higher R^2 (0.92 and 0.95) (Cao et al. 2020). According to assumption of pseudo-second-order model, the adsorption rate is closely related to the number of available adsorption sites on the surface of adsorbent, indicating that the adsorption of phosphate on SRB 2:1 could be

mainly related to the chemisorptions (Guo et al. 2021), electrostatic attraction (Shakya and Agarwal 2019), surface precipitation and ligand exchange (Chen et al. 2014).

For the fitting of the intra-particle diffusion model, the adsorption process of phosphate could be divided into two parts, consisting of external and internal diffusion (Wang et al. 2017). Seen from Table 3, the R^2 was in the range of 0.90–0.99, which showed that the adsorption process of SRB 2:1 was consistent with the intra-particle diffusion model. At the first region, the k_{i1} values of phosphate (100 mg P/L and 200 mg P/L) were 2.3 and 2.9 mg g^{-1} $min^{-1/2}$, respectively. It showed that phosphate sorption rate was high, which was mainly attributed to abundant adsorption sites on the surface of SRB 2:1. After the saturation of external adsorption sites, the diffusion process started to shift into internal diffusion of the second region with low adsorption rate, and the k_{i2} values reduced to 0.29 and 1.18 mg g^{-1} $min^{-1/2}$, respectively. After phosphate diffused into the internal space of SRB 2:1, it formed precipitation with less Ca^{2+}, resulting in the decrease of adsorption rate. In addition, the intercept distance (C_{i1} and C_{i2}) clearly expanded from the first region to the second region, which suggested that the adsorption process was resisted by the boundary layer and controlled by the intra-particle diffusion (Xi et al. 2021).

Adsorption thermodynamic

The adsorption thermodynamic experiment of phosphate was conducted to determine the relationship between temperature variation and adsorption reaction of phosphate on SRB 2:1. The parameters of thermodynamic are presented in Table 4. The relation between $1/T$ and $\ln K_d$ is presented in Online Resource 5. The thermodynamic formulas are as follows:

$$\Delta G^{\circ} = -RT\ln K_d \tag{6}$$

$$\ln K_d = \Delta S^{\circ}/R - \Delta H^{\circ}/RT \tag{7}$$

where K_d is a parameter that represents the thermodynamic equilibrium; ΔH°, ΔS° and ΔG° express the change values about enthalpy, entropy and free energy, respectively; $R = 8.314$; and T refers to the external temperature.

Seen from Online Resource 5a, the adsorption ability of phosphate on SRB 2:1 showed an ascending trend with the temperature increase. The negative $\Delta G°$ values suggested that the phosphate adsorption process was spontaneous (Borgohain et al. 2020). All values of $\Delta G°$ decreased with temperature increase, indicating that the removal efficiency of phosphate on SRB 2:1 was gradually improved with temperature increase (Liu et al. 2019). The positive enthalpy value ($\Delta H°$) indicated that the adsorption process could be an endothermic reaction. The entropy value ($\Delta S°$) was positive, demonstrating that the randomness of the adsorption reaction and the affinity between SRB 2:1 and phosphate were increased in the adsorption process (Guo et al. 2021).

The effect of co-existing anions

The effect of co-existing anions (i.e., Cl^-, SO_4^{2-}, NO_3^- and HCO_3^-) on phosphate adsorption is shown in Fig. 8. The adsorption capacity of phosphate kept stable when concentrations of Cl^-, NO_3^-, and SO_4^{2-}increased from 0.5 g/L to 4 g/L, suggesting that the three anions (Cl^-, SO_4^{2-}, and NO_3^-) had a little influence on the adsorption of phosphate onto the biochar. However, the presence of HCO_3^-sharply reduced the adsorption capacity from 109 mg P/g to 37 mg P/g, when concentrations of HCO_3^-increased from 0.5 g/L to 4 g/L. This was because the inner-sphere complexes produced between bicarbonate in the solution and metal cations from the surface of biochar can inhibit the formation of Ca-P precipitate on the surface of SRB 2:1 (Yin et al. 2013).

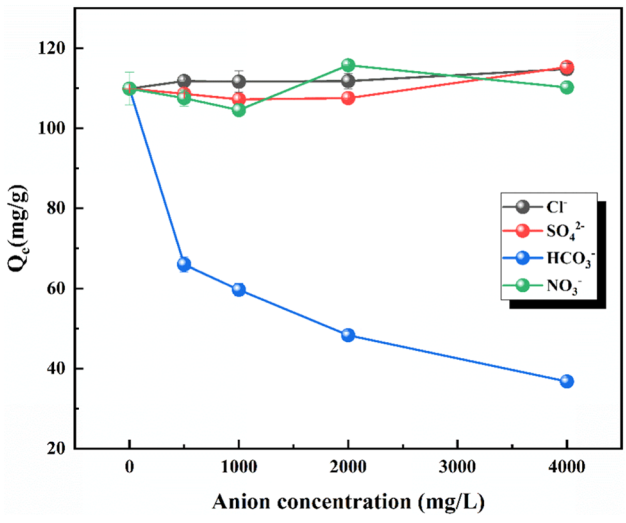

Fig. 8 Effect of co-existing anions for phosphate adsorption on SRB 2:1

Adsorption mechanisms

To explore the mechanism of phosphate adsorption onto SRB 2:1, the analysis of SEM–EDS, FTIR and XRD

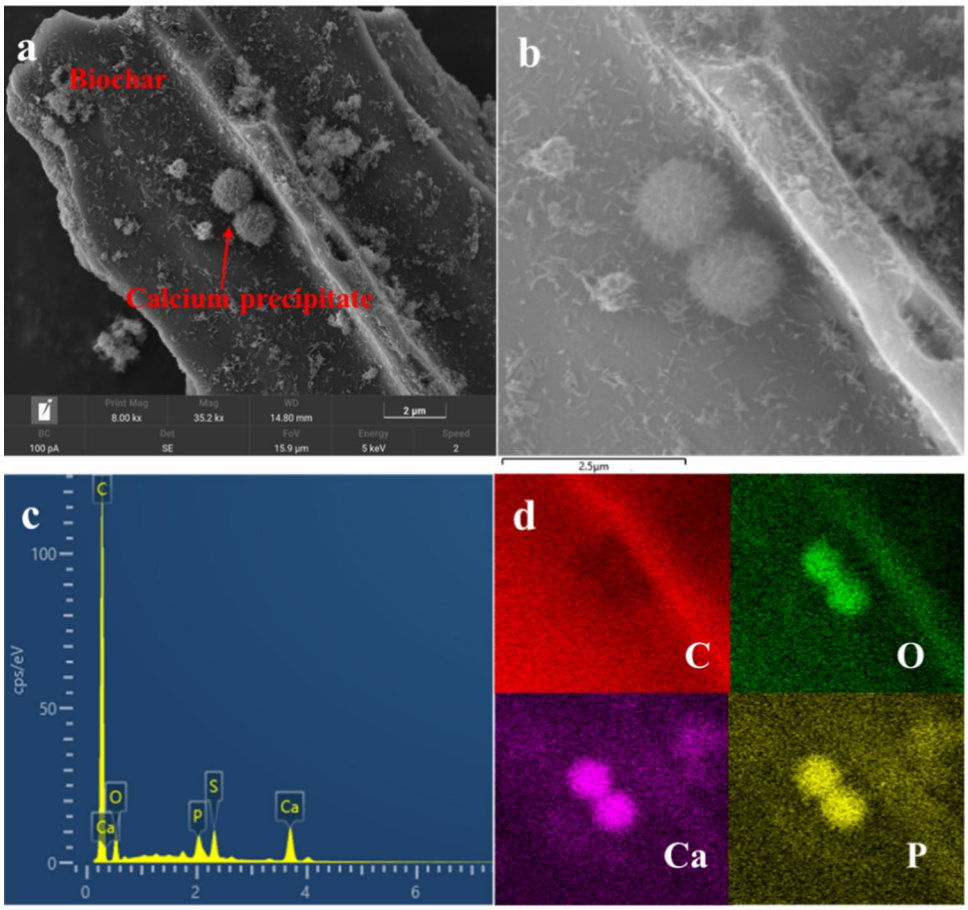

Fig. 9 SEM–EDS images of post-adsorption SRB 2:1 (a, b, c, d)

before and after adsorption was comparatively conducted. According to SEM–EDS analysis, the P content of SRB 2:1 increased significantly and many flocculent crystals attached onto the surface of post-adsorption SRB 2:1, suggesting that phosphate was successfully adsorbed to the surface of modified biochar by the formation of phosphorus-containing compounds. Especially, some spherical particles were observed from Fig. 9a, which was attributed to crystals cluster of hydroxyapatite. Compared with raw SRB 2:1, the new peak emerging at 1055 cm^{-1} belonged to the bending vibration of P–O groups (Fig. 3b). After adsorption, the peaks of CaS and CaO of SRB 2:1 completely disappeared and new peaks at $2\theta = 25.97°$,32°, 39.8°, 46.85, 49.59°, 50.54°, 51.36°, 52.22°, 53.32° and 56.01° appeared, which were ascribed to the typical hydroxyapatite crystals (i.e., $Ca_5(PO_4)_3(OH)$) (Fig. 4b) (Liu et al. 2019; Vahdat et al. 2019; Wang et al. 2018). In addition, a diffraction peak at $2\theta = 34.26°$ represented amorphous calcium phosphate ($Ca_3(PO_4)_2$), which was an unstable calcium-phosphorus compound generated due to the effect of Ca/P and solution pH before hydroxyapatite was formed (Zhuo et al. 2022). Hence, it indicated that the formation of surface precipitate (Eqs. 8–10) between phosphate from the solution and calcium on the surface of SRB 2:1 was the main mechanism to remove phosphate.

$$5Ca^{2+} + 3PO_4^{3-} + OH^- = Ca_5\left(PO_4\right)_3(OH) \downarrow \quad (8)$$

$$5Ca^{2+} + 3HPO_4^{2-} + 4OH^- = Ca_5\left(PO_4\right)_3(OH) \downarrow + 3H_2O \quad (9)$$

$$5Ca^{2+} + 3H_2PO_4^- + 7OH^- = Ca_5\left(PO_4\right)_3(OH) \downarrow + 6H_2O \quad (10)$$

According to the zero potential of SRB 2:1, the surface of modified biochars was positively charged below pH 10.0, thus the electrostatic attraction between SRB 2:1 and negatively charged phosphate was conducive to enhance removal ability of phosphate. With the solution pH increased to over 10.0, phosphate removal was not related to electrostatic attraction due to the electronegativity of modified biochars. The ligand exchange between –OH, –COOH and C=O on the surface of biochar and the unprotonated oxygen atoms in PO_4^{3-} is an important mechanism for biochar to adsorb phosphate (Feng et al. 2022). Meanwhile, according to the

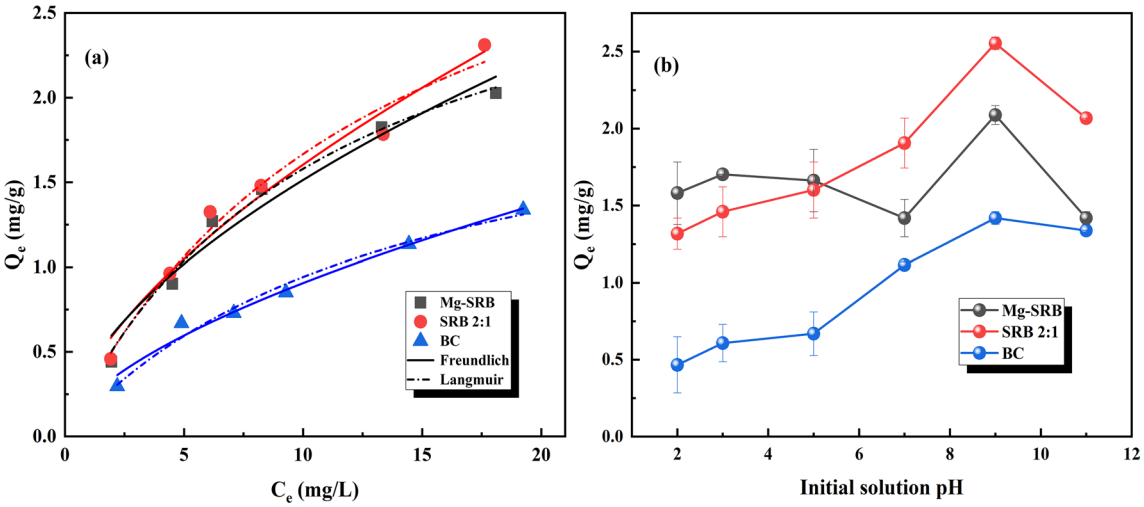

Fig. 10 Adsorption isotherm curves of ammonium onto BC, SRB 2:1 and Mg-SRB at pH 9.0 (**a**); and the effect for removing ammonium at different pH (**b**)

Table 5 Comparison of phosphate and nitrogen removal ability for modified biochars from the literature

Modified biochar	Q_{max} (mg P/g)	Q_{max} (mg N/g)	References
Calcium alginate-biochar	24.1	12.27	Feng et al. (2022)
Mg-doped biochar/bentonite	132.2	39.5	Xi et al. (2022)
Iron- and nitrogen-modified biochar	165.02	111.87	Li and Shi (2022)
Mg-impregnated biochar	136.4	77	Cai and Ye (2022)
K_2CO_3-activated oil palm shell biochar	0.89	1.49	Munar-Florez et al. (2021)
Microalgae-derived nanoporous biochar	–	69	Zhang et al. (2022)
Magnesium-oxide-modified wood waste biochar	116.4	47.5	Xu et al. (2018)
Calcium-modified corn stover biochar	33.94	–	Zhuo et al. (2022)
Acidified magnetic sludge biochar	–	9.67	Wu et al. (2022)
Fe_3O_4 nanoparticles supported sludge biochar	–	1.78	Zhang et al. (2018)
Soda residue-modified sorghum straw biochar	114.96	3.87	This study

analyses of isotherms and kinetics, the adsorption process of phosphate on SRB 2:1 was chemisorption and the adsorption ability of that was dependent on the amount of activated sorption sites on the surface of modified biochars (Xue et al. 2021). After adsorption, no crystal related to magnesium phosphate was found in XRD patterns for P-laden SRB 2:1, which indicated that amorphous phosphate precipitation could form. In conclusion, the main adsorption mechanisms of phosphate on SRB 2:1 were surface precipitation, electrostatic attraction and ligand exchange.

Performance on ammonium (NH_4^+) removal

In addition to phosphate, NH_4^+ is another key pollutant causing the eutrophication of water, so it is important to investigate the removal ability of NH_4^+ onto soda residue-modified biochar. Seen from Fig. 10b, the adsorption

Table 6 Water quality parameters of real domestic wastewater before and after treatment

Test item	Before treatment	After treatment
pH	7.68	9.85
Eh (mV)	− 266	− 232
COD (mg/L)	216	83
TP (mg/L)	4.06	0.17
NH_4^+ (mg/L)	44.0	41.4
NO_3^- (mg/L)	1.51	1.29
PO_4^{3-} (mg/L)	3.14	0.16

ability of NH_4^+ for SRB 2:1 gradually increased with the pH increasing from 2 to 9, possibly due to the electrostatic attraction between modified biochars and NH_4^+ (Ahmad et al. 2014). NH_4^+ was the existing form of ammonium in the acidic aqueous. As the pH of solutions was gradually increased, the amount of H^+ became less, resulting in more positively charged NH_4^+ in the solution combining with carboxylic and hydroxyl groups on the surface of biochars. When the pH of solution exceeded the pH_{pzc} of SRB 2:1, the volatile ammonia molecules were formed via the interaction between OH^- and NH_4^+ in the solution. The surface of the modified biochar was positively charged, thus the adsorption capacities of NH_4^+ reduced, but were still higher than those of the acidic solutions (Ismail and Hameed 2014).

The adsorption isotherms of Mg-SRB, SRB 2:1 and BC are shown in Fig. 10a. All the absorbents exhibited to a certain extent removal ability for NH_4^+. The maximum adsorption capacities of SRB 2:1 and Mg-SRB reached 3.87 mg N/g and 3.30 mg N/g, respectively, which were higher than that of BC (2.27 mg N/g), indicating that soda residue-modified biochars enhanced NH_4^+ removal ability of raw biochar. In previous studies, Zhang et al. (Zhang et al. 2018) prepared the adsorbent with Fe_3O_4 nanoparticles and excessive sludge and exhibited NH_4^+ adsorption capacity of 1.78 mg N/g. Munar-Florez et al. (2021) reported that the oil palm shell biochar was activated by K_2CO_3 to remove NH_4^+ with the Q_m of 1.49 mg N/g. Therefore, the removal capacity of SRB 2:1 was comparable with many materials reported in the literature and it may become potential adsorbent for removing NH_4^+ in water (Table 5).

Treatment of phosphate in real domestic wastewater

The real domestic wastewater was used to further assess the actual application potential of SRB 2:1, and the characteristics of domestic wastewater before and after treatment are listed in Table 6. The results indicated that the concentrations of TP and PO_4^{3-} decreased from 4.06 mg/L to 0.17 mg/L and from 3.14 mg/L to 0.16 mg/L, respectively, and the phosphate removal rates of them reached 95.8% and 94.9%, meeting the phosphate discharge standard (0.5 mg/L) in wastewater (Li and Shi 2022). Besides, the concentrations of NH_4^+ and NO_3^- declined from 44.0 mg/L to 41.4 mg/L and from 1.51 mg/L to 1.29 mg/L, respectively, suggesting that the modified biochar possessed removal ability for NH_4^+ and NO_3^-. It is worth noting that the pH of the treated sewage reached above 9, which exceeds the requirements of integrated wastewater discharge standard in China (6–9). Therefore, the treatment of acidic wastewater may have priority and advantages.

Pot experiment: nutrients recovery

Seen form Online Resource 6(a), in view of height and quantity of blades and roots, the growth of wheat in different soils could be ranked: blank < commercial fertilizer < SRB 2:1 < post-adsorption SRB 2:1. It indicated that post-adsorption SRB 2:1 improved the growth of wheat seedlings to a certain extent. Seen from Online Resource 6(b), the measurement indicators of post-adsorption SRB 2:1 were higher than those of other groups after the wheat seedlings were harvested, which was consistent with the intuitive results of Online Resource 6(a). Owing to the presence of hydroxyapatite ($Ca_5(PO_4)_3(OH)$) and nitrogen in post-adsorption SRB 2:1, the crop growth situation was better than that of other groups with less phosphorus and nitrogen. SRB 2:1 material containing mineral elements (e.g., Ca, Mg, Si) also promoted growth of wheat seedlings, which was only lower than post-adsorption SRB 2:1. The results indicated that post-adsorption-modified biochar could have the potential to replace chemical fertilizer to be used as slow-releasing fertilizer.

With the completion of pot experiment, the physicochemical properties (pH and EC) of soils were surveyed to reveal the effect of post-adsorption biochar for the soil quality (Online Resource 6(c)). Compared with raw soil (pH = 7.5, EC = 375 μS/cm), the pH and EC of soil which was added post-adsorption SRB 2:1 increased to 8.62 and 380 μS/cm, respectively, which could be attributed to the high pH (Table 1) and ion-rich composition of modified biochar. High alkalinity of soil may affect the growth of some kinds of crop. Hence, it is necessary to evaluate their effectiveness for different crops in the future and long-term potential impact for soil quality. Furthermore, it is recommended using wastewater recovered nutrients (post-adsorption biochar) as forest and grassland fertilizer rather than farmland to produce grain and vegetable.

Conclusion

A novel soda residue-modified straw biochar composite (SRB 2:1) was prepared for efficient recovery of phosphate and ammonium from water. The maximum adsorption

capacity of SRB 2:1 toward phosphate and ammonium were about 80 and 1.7 times that of raw straw biochar, respectively. The adsorption mechanisms of removing phosphate on SRB 2:1 mainly included surface precipitation (hydroxyapatite), ligand exchange and electrostatic adsorption. It exhibited excellent performance on removing nutrients from real domestic wastewater, particularly with 95% removal for phosphate. Pot experiment indicated that post-adsorption SRB 2:1 as a slow-releasing fertilizer promoted growth of wheat seedlings. The soda residue as a novel modifier of biochar could improve the recovery of phosphate and ammonium, which not only achieved the recycling of solid waste, but also reduced the production cost of biochar adsorbent.

Supplementary Information The online version contains supplementary material available at https://doi.org/10.1007/s13762-023-04935-4.

Acknowledgements The authors wish to thank all who assisted in conducting this work.

Declarations

Conflict of interest The authors declare that they have no known competing financial interests or personal relationships that could have appeared to influence the work reported in this paper.

Ethical approval This article does not contain any studies with human participants or animals performed by any of the authors.

References

Ahmad M, Lee SS, Dou X, Mohan D, Sung J-K, Yang JE, Ok YS (2012) Effects of pyrolysis temperature on soybean stover- and peanut shell-derived biochar properties and TCE adsorption in water. Biores Technol 118:536–544

Ahmad M, Rajapaksha AU, Lim JE, Zhang M, Bolan N, Mohan D, Vithanage M, Lee SS, Ok YS (2014) Biochar as a sorbent for contaminant management in soil and water: a review. Chemosphere 99:19–33

Amin M, Chetpattananondh P (2019) Biochar from extracted marine Chlorella sp residue for high efficiency adsorption with ultrasonication to remove Cr(VI), Zn(II) and Ni(II). Bioresour Technol 289:121578

An Q, Li Z, Zhou Y, Meng F, Zhao B, Miao Y, Deng S (2021) Ammonium removal from groundwater using peanut shell based modified biochar: mechanism analysis and column experiments. J Water Process Eng 43:102219

Banu HT, Karthikeyan P, Meenakshi S (2019) Zr^{4+} ions embedded chitosan-soya bean husk activated bio-char composite beads for the recovery of nitrate and phosphate ions from aqueous solution. Int J Biol Macromol 130:573–583

Borgohain X, Boruah A, Sarma GK, Rashid MH (2020) Rapid and extremely high adsorption performance of porous MgO nanostructures for fluoride removal from water. J Mol Liq 305:112799

Cai G, Ye Z-l (2022) Concentration-dependent adsorption behaviors and mechanisms for ammonium and phosphate removal by optimized Mg-impregnated biochar. J Clean Prod 349:131453

Cao H, Wu X, Syed-Hassan SSA, Zhang S, Mood SH, Milan YJ, Garcia-Perez M (2020) Characteristics and mechanisms of phosphorous adsorption by rape straw-derived biochar functionalized with calcium from eggshell. Biores Technol 318:124063

Chen N, Feng C, Zhang Z, Liu R, Gao Y, Li M, Sugiura N (2012) Preparation and characterization of lanthanum(III) loaded granular ceramic for phosphorus adsorption from aqueous solution. J Taiwan Inst Chem Eng 43:783–789

Chen T, Zhang Y, Wang H, Lu W, Zhou Z, Zhang Y, Ren L (2014) Influence of pyrolysis temperature on characteristics and heavy metal adsorptive performance of biochar derived from municipal sewage sludge. Biores Technol 164:47–54

Duan X, Sun H, Wang Y, Kang J, Wang S (2015) N-doping-induced nonradical reaction on single-walled carbon nanotubes for catalytic phenol oxidation. ACS Catal 5:553–559

Fang Q, Chen B, Lin Y, Guan Y (2014) Aromatic and hydrophobic surfaces of wood-derived biochar enhance perchlorate adsorption via hydrogen bonding to oxygen-containing organic groups. Environ Sci Technol 48:279–288

Feng Q, Chen M, Wu P, Zhang X, Wang S, Yu Z, Wang B (2022) Simultaneous reclaiming phosphate and ammonium from aqueous solutions by calcium alginate-biochar composite: Sorption performance and governing mechanisms. Chem Eng J 429:132166

Guo N, Lv X, Yang Q, Xu X, Song H (2021) Effective removal of hexavalent chromium from aqueous solution by ZnCl2 modified biochar: effects and response sequence of the functional groups. J Mol Liq 334:116149

Ismail ZZ, Hameed BB (2014) A new application of giant reed waste material for ammonium removal. Int J Environ Stud 71:122–138

Kong L, Han M, Shih K, Su M, Diao Z, Long J, Chen D, La H, Peng Y (2018) Nano-rod Ca-decorated sludge derived carbon for removal of phosphorus. Environ Pollut 233:698–705

Li X, Shi J (2022) Simultaneous adsorption of tetracycline, ammonium and phosphate from wastewater by iron and nitrogen modified biochar: kinetics, isotherm, thermodynamic and mechanism. Chemosphere 293:133574

Li J, Li B, Huang H, Lv X, Zhao N, Guo G, Zhang D (2019) Removal of phosphate from aqueous solution by dolomite-modified biochar derived from urban dewatered sewage sludge. Sci Total Environ 687:460–469

Li X, Wang C, Zhang J, Liu J, Liu B, Chen G (2020) Preparation and application of magnetic biochar in water treatment: A critical review. Sci Total Environ 711:134847

Lian G, Wang B, Lee X, Li L, Liu T, Lyu W (2019) Enhanced removal of hexavalent chromium by engineered biochar composite fabricated from phosphogypsum and distillers grains. Sci Total Environ 697:134119

Liu X, Shen F, Qi X (2019) Adsorption recovery of phosphate from aqueous solution by CaO-biochar composites prepared from eggshell and rice straw. Sci Total Environ 666:694–702

Ma Y, Yang L, Wu L, Li P, Qi X, He L, Cui S, Ding Y, Zhang Z (2020) Carbon nanotube supported sludge biochar as an efficient adsorbent for low concentrations of sulfamethoxazole removal. Sci Total Environ 718:137299

McGinley J, Healy MG, Ryan PC, Mellander PE, Morrison L, O'Driscoll JH, Siggins A (2022) Batch adsorption of herbicides from aqueous solution onto diverse reusable materials and granulated activated carbon. J Environ Manage 323:116102

Mia S, Dijkstra FA, Singh B (2017) Aging induced changes in biochar's functionality and adsorption behavior for phosphate and ammonium. Environ Sci Technol 51:8359–8367

Mitrogiannis D, Psychoyou M, Baziotis I, Inglezakis VJ, Koukouzas N, Tsoukalas N, Palles D, Kamitsos E, Oikonomou G, Markou G (2017) Removal of phosphate from aqueous solutions by adsorption onto $Ca(OH)_2$ treated natural clinoptilolite. Chem Eng J 320:510–522

Munar-Florez DA, Varón-Cardenas DA, Ramírez-Contreras NE, García-Núñez JA (2021) Adsorption of ammonium and phosphates by biochar produced from oil palm shells: effects of production conditions. Results Chem 3:100119

Phuong Tran TC, Nguyen TP, Nguyen TT, Le PC, Tran QB, Nguyen XC (2022) Equilibrium single and co-adsorption of nutrients from aqueous solution onto aluminium-modified biochar. Case Stud Chem Environ Eng 5:100181

Qi Y, Guo C, Xu X, Gao B, Yue Q, Jiang B, Qian Z, Wang C, Zhang Y (2020) Co/Fe and Co/Al layered double oxides ozone catalyst for the deep degradation of aniline: preparation, characterization and kinetic model. Sci Total Environ 715:136982

Qiu B, Duan F (2019) Synthesis of industrial solid wastes/biochar composites and their use for adsorption of phosphate: from surface properties to sorption mechanism. Colloids Surf, A 571:86–93

Shakoor MB, Ye Z-L, Chen S (2021) Engineered biochars for recovering phosphate and ammonium from wastewater: a review. Sci Total Environ 779:146240

Shakya A, Agarwal T (2019) Removal of Cr (VI) from water using pineapple peel derived biochars: Adsorption potential and reusability assessment. J Mol Liq 293:111497

Sing KSW (1982) Reporting physisorption data for gas/solid systems with special reference to the determination of surface area and porosity (Provisional). Pure Appl Chem 54:2201–2218

Tian Y, Li J, Whitcombe TW, McGill WB, Thring R (2020) Application of oily sludge-derived char for lead and cadmium removal from aqueous solution. Chem Eng J 384:123386

Vahdat A, Ghasemi B, Yousefpour M (2019) Synthesis of hydroxyapatite and hydroxyapatite/Fe3O4 nanocomposite for removal of heavy metals. Environ Nanotechnol Monitor Manag 12:100233

Wang H, Wang X, Ma J, Xia P, Zhao J (2017) Removal of cadmium (II) from aqueous solution: a comparative study of raw attapulgite clay and a reusable waste–struvite/attapulgite obtained from nutrient-rich wastewater. J Hazard Mater 329:66–76

Wang S, Kong L, Long J, Su M, Diao Z, Chang X, Chen D, Song G, Shih K (2018) Adsorption of phosphorus by calcium-flour biochar: isotherm, kinetic and transformation studies. Chemosphere 195:666–672

Wang B, Lian G, Lee X, Gao B, Li L, Liu T, Zhang X, Zheng Y (2020) Phosphogypsum as a novel modifier for distillers grains biochar removal of phosphate from water. Chemosphere 238:124684

Wang B, Ma Y, Lee X, Wu P, Liu F, Zhang X, Li L, Chen M (2021) Environmental-friendly coal gangue-biochar composites reclaiming phosphate from water as a slow-release fertilizer. Sci Total Environ 758:143664

Wu R, Zhai X, Dai K, Lian J, Cheng L, Wang G, Li J, Yang C, Yin Z, Li H, Yang X (2022) Synthesis of acidified magnetic sludge-biochar and its role in ammonium nitrogen removal: Perception on effect and mechanism. Sci Total Environ 832:154780

Xi H, Li Q, Yang Y, Zhang J, Guo F, Wang X, Xu S, Ruan S (2021) Highly effective removal of phosphate from complex water environment with porous Zr-bentonite alginate hydrogel beads: facile synthesis and adsorption behavior study. Appl Clay Sci 201:105919

Xi H, Zhang X, Hua Zhang A, Guo F, Yang Y, Lu Z, Ying G, Zhang J (2022) Concurrent removal of phosphate and ammonium from wastewater for utilization using Mg-doped biochar/bentonite composite beads. Sep Purif Technol 285:120399

Xu R, Zhang M, Mortimer RJG, Pan G (2017) Enhanced phosphorus locking by novel lanthanum/aluminum–hydroxide composite: implications for eutrophication control. Environ Sci Technol 51:3418–3425

Xu K, Lin F, Dou X, Zheng M, Tan W, Wang C (2018) Recovery of ammonium and phosphate from urine as value-added fertilizer using wood waste biochar loaded with magnesium oxides. J Clean Prod 187:205–214

Xu K, Li L, Huang Z, Tian Z, Li H (2022) Efficient adsorption of heavy metals from wastewater on nanocomposite beads prepared by chitosan and paper sludge. Sci Total Environ 846:157399

Xue J, Wang H, Li P, Zhang M, Yang J, Lv Q (2021) Efficient reclaiming phosphate from aqueous solution using waste limestone modified sludge biochar: mechanism and application as soil amendments. Sci Total Environ 799:149454

Yao Y, Gao B, Chen J, Yang L (2013) Engineered biochar reclaiming phosphate from aqueous solutions: mechanisms and potential application as a slow-release fertilizer. Environ Sci Technol 47:8700–8708

Yin H, Kong M, Fan C (2013) Batch investigations on P immobilization from wastewaters and sediment using natural calcium rich sepiolite as a reactive material. Water Res 47:4247–4258

Zhang Q, Du Q, Jiao T, Pan B, Zhang Z, Sun Q, Wang S, Wang T, Gao F (2013) Selective removal of phosphate in waters using a novel of cation adsorbent: zirconium phosphate (ZrP) behavior and mechanism. Chem Eng J 221:315–321

Zhang L-J, Zhang X, Liang H-F, Xie Y, Tao H-C (2018) Ammonium removal by a novel magnetically modified excess sludge. Clean Technol Environ Policy 20:2181–2189

Zhang M, Song G, Gelardi DL, Huang L, Khan E, Mašek O, Parikh SJ, Ok YS (2020a) Evaluating biochar and its modifications for the removal of ammonium, nitrate, and phosphate in water. Water Res 186:116303

Zhang T, Wu X, Shaheen SM, Zhao Q, Liu X, Rinklebe J, Ren H (2020b) Ammonium nitrogen recovery from digestate by hydrothermal pretreatment followed by activated hydrochar sorption. Chem Eng J 379:122254

Zhang Y, Liu N, Yang Y, Li J, Wang S, Lv J, Tang R (2020c) Novel carbothermal synthesis of Fe, N co-doped oak wood biochar (Fe/N-OB) for fast and effective Cr(VI) removal. Colloids Surf, A 600:124926

Zhang Y, Akindolie MS, Tian X, Wu B, Hu Q, Jiang Z, Wang L, Tao Y, Cao B, Qu J (2021) Enhanced phosphate scavenging with effective recovery by magnetic porous biochar supported $La(OH)_3$: kinetics, isotherms, mechanisms and applications for water and real wastewater. Biores Technol 319:124232

Zhang H, Song Y, Liu Y, Zhao J, Li Y (2022) First-principles study of sodium adsorption and diffusion on vacancies, N, S, and NS-codoped graphene. Mater Today Commun 32:103817

Zhao L, Zhao Y, Nan H, Yang F, Qiu H, Xu X, Cao X (2020) Suppressed formation of polycyclic aromatic hydrocarbons (PAHs) during pyrolytic production of Fe-enriched composite biochar. J Hazard Mater 382:121033

Zhuo S-N, Dai T-C, Ren H-Y, Liu B-F (2022) Simultaneous adsorption of phosphate and tetracycline by calcium modified corn stover biochar: performance and mechanism. Biores Technol 359:127477